symmetry

MDPI

Article

$AgGaGeSe_4$: An Infrared Nonlinear Quaternary Selenide with Good Performance

Junhui Dang [1], Naizheng Wang [2], Jiyong Yao [2], Yuandong Wu [1], Zheshuai Lin [2] and Dajiang Mei [1,3,*]

[1] College of Chemistry and Chemical Engineering, Shanghai University of Engineering Science, Shanghai 201620, China; dangjh2022@163.com (J.D.); wuyuandong@sues.edu.cn (Y.W.)
[2] Technical Institute of Physics and Chemistry, Chinese Academy of Sciences, Beijing 100190, China; wnzheng@163.com (N.W.); jyao@mail.ipc.ac.cn (J.Y.); zslin@mail.ipc.ac.cn (Z.L.)
[3] State Key Laboratory of Structural Chemistry, Fujian Institute of Research on the Structure of Matter, Chinese Academy of Sciences, Fuzhou 350002, China
* Correspondence: meidajiang718@pku.edu.cn

Abstract: The symmetry of crystals is an extremely important property of crystals. Crystals can be divided into centrosymmetric and non-centrosymmetric crystals. In this paper, an infrared (IR) nonlinear optical (NLO) material $AgGaGeSe_4$ was synthesized. The related performance analysis, nonlinear optical properties, and first-principle calculation of $AgGaGeSe_4$ were also introduced in detail. In the $AgGaGeSe_4$ structure, Ge^{4+} was replaced with Ga^{3+} and produced the same number of vacancies at the Ag^+ position. The low content of Ge doping kept the original chalcopyrite structure and improved its optical properties such as the band gap. The UV-Vis diffuse reflection spectrum shows that the experimental energy band gap of $AgGaGeSe_4$ is 2.27 eV, which is 0.48 eV larger than that of $AgGaSe_2$ (1.79 eV). From the perspective of charge-transfer engineering strategy, the introduction of Group IV Ge elements into the crystal structure of $AgGaSe_2$ effectively improves its band gap. The second harmonic generation (SHG) effect of $AgGaGeSe_4$ is similar to that of $AgGaSe_2$, and at 1064 nm wavelength, the birefringence of $AgGaGeSe_4$ is 0.03, which is greater than that of $AgGaSe_2$ (Δn = 0.02). The results show that $AgGaGeSe_4$ possessed better optical properties than $AgGaSe_2$, and can been broadly applied as a good infrared NLO material.

Keywords: nonlinear optical crystal; crystal structure; optical properties

check for updates

Citation: Dang, J.; Wang, N.; Yao, J.; Wu, Y.; Lin, Z.; Mei, D. $AgGaGeSe_4$: An Infrared Nonlinear Quaternary Selenide with Good Performance. *Symmetry* **2022**, *14*, 1426. https://doi.org/10.3390/sym14071426

Academic Editor: Enrique Maciá Barber

Received: 14 February 2022
Accepted: 1 June 2022
Published: 12 July 2022

1. Introduction

Infrared lasers have been widely used in the civil and military fields and are generally obtained by converting the frequency of a laser light source from infrared nonlinear optical materials [1–6]. With the development of science and technology, infrared nonlinear optical crystal materials have been popularized in the applications. Demand for the requirements of infrared nonlinear optical crystal materials has emerged in the practical use. At present, many crystals can achieve frequency conversion in principle, but in fact, only few crystals, such as $AgGaS_2$, $AgGaSe_2$, and $ZnGeP_2$, are commercially mature [7–9]. Although the application of chalcopyrite infrared crystals has been promoted via the progress of high-quality crystal growth and processing technology, these infrared crystals still have shortcomings in terms of their properties, for instance, the low laser damage threshold of $AgGaS_2$ and $AgGaSe_2$, the small band gap of $AgGaSe_2$ (1.79 eV), and the serious two-photon absorption of $ZnGeP_2$ [10–12]. All these existing problems limit their wide application.

Generally, the second harmonic generation is generated by non-centrosymmetric crystals, and a large energy band gap benefits from improving the laser damage threshold and the transparency of nonlinear optical crystals [13–15]. This is not only of great significance to the functional optimization of infrared nonlinear optical crystals but also has an important impact on the reasonable structural design of other functional materials with

a broad band gap [16–21]. Therefore, the exploration of infrared nonlinear optical crystal materials with excellent properties, such as large band gap, high laser damage threshold, and good nonlinear optical effect, remains challenging [22–25]. In order to overcome this problem, researchers have carried out a lot of experimental exploration work. Through continuous exploration and research, it is found that the introduction of lighter Group IV Si and Ge elements can effectively enhance their band gap [26–37]. For example, the energy band gap of the synthesized $Ag_3Ga_3SiSe_8$ compound is 2.30 eV, which is larger than that of $AgGaSe_2$ [38]. The energy band gap of the synthesized $AgGaGe_5Se_{12}$ compound is 2.20 eV, which is larger than that of $AgGaSe_2$ [39,40].

In 1980, O.H. Hughes et al. synthesized $AgGaGeSe_4$ powder by adding the Ge element on the basis of $AgGaSe_2$ [41]. However, there is no comprehensive investigation of the synthesis of $AgGaGeSe_4$ crystal and its related performance analysis, nonlinear optical properties, and first-principle calculation. In this work, the $AgGaGeSe_4$ crystal with a tetragonal chalcopyrite structure was synthesized by introducing lighter Group IV Ge elements in the $AgGaSe_2$ crystal, and the corresponding performance was tested and analyzed. The nonlinear optical properties and first-principle calculation were also investigated in detail. In addition, the band gap of $AgGaGeSe_4$ was analyzed and discussed by using a charge-transfer engineering strategy.

2. Experimental Section

2.1. Synthetic Samples

The synthesis of $AgGaGeSe_4$ powder samples consists of two steps. In the first step, ternary $AgGaSe_2$ and binary $GeSe_2$ were prepared by high-temperature solid-state synthesis technology with Ag 99.9%, Ga 99.9%, Ge 99.9%, and Se 99.9% as raw materials. The elements were loaded into silica glass tubes with the required stoichiometry and sealed with hydrogen at a vacuum pressure of less than 10^{-3} Pa. The annealing temperature of $AgGaSe_2$ was 900 °C and that of $GeSe_2$ was 680 °C. The second step is to mix an appropriate amount of $AgGaSe_2$ and $GeSe_2$ in a molar ratio of 1:1 in a glove box filled with argon, put them into a silica glass tube, and seal them with hydrogen under a vacuum pressure of less than 10^{-3} Pa. Then, put them into a computer-controlled muffle furnace, set the program to heat it to 950 °C for 20 h, keep it at this temperature for 10 h, and then cool it to room temperature. The reaction was repeated three times and ground intermittently to synthesize the quaternary compound of $AgGaGeSe_4$.

2.2. Single Crystal Growth

Mix an appropriate amount of $AgGaSe_2$ and $GeSe_2$ in a molar ratio of 1:1 in a glove box filled with argon, put them into a silica glass tube, and seal them with hydrogen under a vacuum pressure of less than 10^{-3} Pa. Then, put them into the computer-controlled muffle furnace, set the program to heat it to 900 °C for 20 h, keep it at this temperature for 24 h, cool it to 600 °C at the rate of 3 °C per hour, and then cool it to room temperature to obtain the single crystal of $AgGaGeSe_4$.

2.3. Determination of Crystal Structure

A high-quality single crystal was firstly selected under an electron microscope. The crystal structure data of $AgGaGeSe_4$ was collected and analyzed by using a Bruker single-crystal diffractometer (Billerica, MA, USA) equipped with graphite-monochromatized Mo Kα radiation (λ = 0.71073 Å). It should be noted that the voltage and current of the X-ray tube were set at 50 kV and 30 mA, respectively. The SHELXTL [42,43] software package (Cambridge, UK) was used to solve the crystal structure directly, and the matrix least square method was used to refine the structure of $AgGaGeSe_4$. The related crystal structure data and specific details are summarized in Tables S1 and S2.

2.4. Energy Dispersive X-ray Spectrometer

Energy dispersive X-ray spectrometer (EDS) testing was performed on an Oxford NT 80 instrument (Oxford, UK), and the result showed that the atomic ratio of Ag, Ga, Ge, and Se in $AgGaGeSe_4$ are 14.59%, 17.42%, 14.94%, and 53.06% (Figure S1).

2.5. UV-Vis Diffuse Reflectance Spectroscopy Analysis

The diffuse reflectance spectra of the $AgGaGeSe_4$ powder were tested by a Shimadzu UV-3600 spectrophotometer (Shimadzu, Kyoto, Japan) with a test range of 200–1500 nm. $BaSO_4$ powder was chosen to be the 100% reflectance standard.

2.6. Second Harmonic Generation Measurement

A 2 μm Q-switch laser was used to measure the SHG response of the $AgGaGeSe_4$ power sample with a particle size of 70–90 μm by the Kurtz–Perry method. At the same time, the reference material was a powder sample of $AgGaSe_2$ with the same particle size.

2.7. X-ray Photoelectron Spectroscopy (XPS)

Use Al Kα (hv = 1487 eV), accept XPS with an average of 5 scans and an energy step of 0.05 eV, collect XPS data under the acceleration voltage of 13 kv and the emission current of 9 mA, and take the carbon signal with a binding energy of 284.8 eV as the reference for displacement correction. The XPS survey scan data of $AgGaGeSe_4$ is shown in Figure S2 and Table S3.

2.8. Theoretical Calculation

We optimized the structure using the first-principle calculation method. The first-principle calculation of the electronic structures in $AgGaGeSe_4$ were performed by the plane-wave pseudopotential method implemented in the CASTEP [44] package based on the density functional theory (DFT) [45,46]. The Perdew–Burk–Ernzerhorf (PBE) function of the general gradient approximation (GGA) and the local density approximation (LDA) Ceperley–Alder (CA) approach form was used to describe the exchange-correlation energy [47–49]. To deal with the interaction between the atomic kernel and valence electrons accurately, the optimized norm-conserving pseudopotential [50] was chosen. Ag $5s^1 4d^{10}$, Ga $4s^2 4p^1 3d^{10}$, Ge $4s^2 4p^{2,}$ and Se $4s^2 4p^4$ were treated as valence electrons, which allowed us to employ a relatively small basis set without compromising the computational accuracy. The kinetic energy cutoff 650 eV and the intensive Monkhorst–Pack [51] k-points 2 × 2 × 2 mesh guarantee the reliability of our results. The refractive index (n) was determined using the Kramers–Kronig transform [52].

3. Results and Discussion

3.1. Crystal Structure

$AgGaGeSe_4$ has a a tetragonal chalcopyrite structure ($I\bar{4}2d$) and is a non-centrosymmetric crystal with second harmonic generation. The cell parameters of $AgGaGeSe_4$ are a = 5.8056(5) Å, $\alpha = 90°$, b = 5.8056(5) Å, $\beta = 90°$, c = 10.3488(10) Å, and $\gamma = 90°$, V = 348.81(7) $Å^3$. The crystal structure diagram is shown in Figure 1. In this structure, Ge^{4+} replaces $Ga^{3+,}$ and an equivalent number of vacancies were generated at the Ag^+ position [53,54]. Then, Ag^+ was rearranged and filled in the tetrahedral vacancy to complete the charge compensation mechanism. Ag atoms and Ge/Ga atoms are, respectively, connected with four Se atoms to form $AgSe_4$ and $(Ge/Ga)Se_4$ tetrahedral structures, and then $AgSe_4$ and $(Ge/Ga)Se_4$ tetrahedrons are connected through common vertices to form a three-dimensional frame structure.

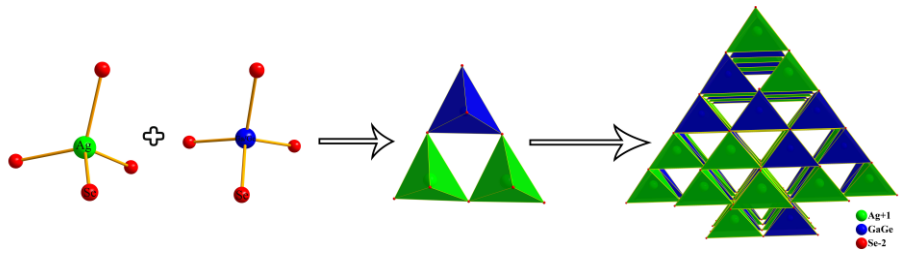

Figure 1. The structure of $AgGaGeSe_4$.

3.2. Powder XRD Pattern

The XRD patterns of polycrystalline products were collected by using the automatic Bruker D2-206918 X-ray diffractometer. XRD simulation was carried out by findit software. According to the single-crystal crystallographic data of $AgGaGeSe_4$, the powder X-ray diffraction pattern obtained from the experiment coincided quite well with the simulated pattern (Figure 2).

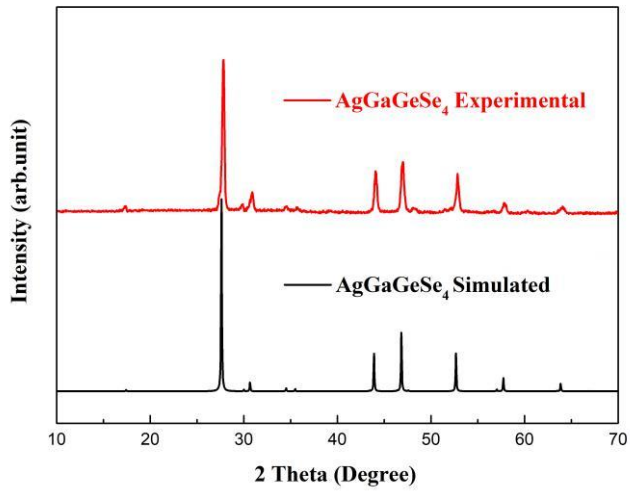

Figure 2. The powder X-ray diffraction patterns of $AgGaGeSe_4$.

3.3. Optical Properties

The band gap of $AgGaGeSe_4$ was measured by the UV-Vis diffuse reflection method. As shown in Figure 3, the diffuse spectrum of $AgGaGeSe_4$ using the upper tangent method [55,56] has a band gap of $AgGaGeSe_4$ is 2.27 eV, and its absorption edge is 546 nm. In addition, the direct band gap of $AgGaGeSe_4$ obtained by the Tauc method was 2.01 eV (Figure S3), which was larger than that of commercial $AgGaSe_2$ (1.79 eV) and larger than that of Kim et al. [26] 1.862 eV and Goodchild et al. [27] 1.85 eV. This may be related to different test methods and different sample purities. Obviously, introducing light Group IV Ge elements into the crystal structure of $AgGaSe_2$ effectively improved the band gap of $AgGaGeSe_4$. It is widely acknowledged that the energy band gap of crystals is closely related to the laser damage threshold and approximately matches the exponential relationship. The large band gap generally helps to improve the laser damage of crystal materials and avoid two-photon absorption. Our results showed that the optical properties of the crystal were significantly enhanced compared with $AgGaSe_2$. $AgGaGeSe_4$ may have a larger laser damage threshold and can be potentially applied in the field of nonlinear optics.

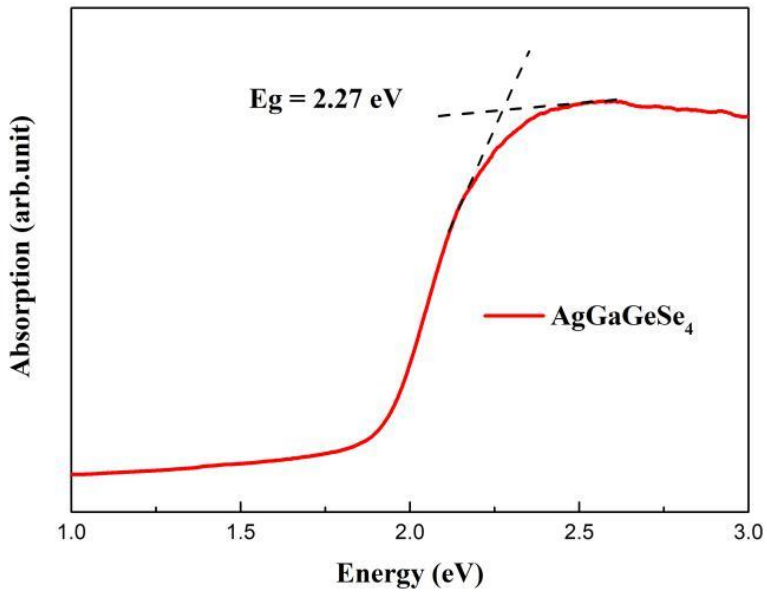

Figure 3. The diffuse spectrum of $AgGaGeSe_4$ using the upper tangent method.

The SHG intensity comparison between the $AgGaGeSe_4$ sample and $AgGaSe_2$ were conducted by using a 2.0 μm laser radiation. The test results showed that $AgGaGeSe_4$ has a similar SHG effect to $AgGaSe_2$ (Figure S4). This can be ascribed to the fact that $AgGaGeSe_4$ and $AgGaSe_2$ have a similar three-dimensional dense structure.

3.4. Theoretical Calculation and Analysis

The band gaps of $AgGaGeSe_4$ calculated by the general gradient approximation (GGA) and the local density approximation (LDA) Ceperley–Alder (CA) approach are 1.207 eV (Figure 4) and 1.25 eV (Figure S5), respectively. The calculation results of the two methods are similar and are lower than the experimentally measured band gap (2.27 eV). Meanwhile, Figure 5 showed the projected density of states (DOS) and the partial density of states (PDOS) of the constituent atoms of $AgGaGeSe_4$. The results demonstrated that the top of the valence band (VB) of $AgGaGeSe_4$ is occupied by the hybrid orbitals of Ag (4*d*) and Se (4*p*). The bottom of the conduction band (CB) consists entirely of atomic orbitals (Ag (5*s*), Ga (4*s*4*p*), Ge (4*s*4*p*), and Se (4*s*4*p*) orbitals). Therefore, the band gap of the $AgGaGeSe_4$ crystal can be evaluated by the electronic transitions in Ag-Se and (Ge/Ga)-Se groups. In $AgGaSe_2$, the Ag 4*d* orbital is located at the top of the valence band (the energy of the 4d orbital is from ~−5.0 to ~−2.0), which increases the maximum energy level of the valence band. Compared with $AgGaGeSe_4$, the Ag orbital is located in the deeper valence band (the energy of 4*d* orbital is from ~−4.0 to ~−3.0), which has no effect on the band gap. From the perspective of atomic electronegativity and the charge-transfer engineering strategy, the band gap of $AgGaGeSe_4$ was determined by an electrostatic interaction between an anion Se^{2-} and two cations Ag^{+} and Ge^{4+}, and the induction effect of Ge on Ag-Se bond can be qualitatively evaluated by the electronegativity difference between Ag and Ge. The electronegativity of Ge (about 2.01) is greater than that of Ag (about 1.90); this led to the charge transfer from $AgSe_4$ tetrahedron to $(Ge/Ga)Se_4$ tetrahedron, which weakened the covalence of Ge-Se bond and increased the band gap of $AgGaGeSe_4$. Therefore, the band gap of $AgGaGeSe_4$ is larger than that of $AgGaSe_2$.

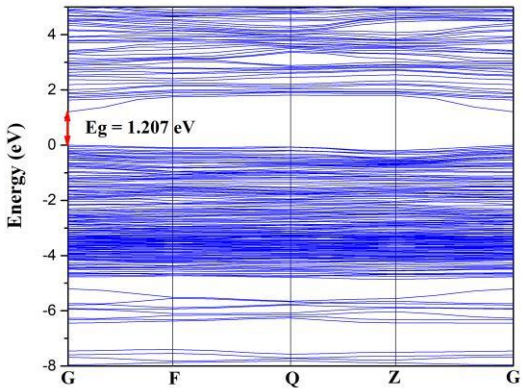

Figure 4. The calculated band structure of $AgGaGeSe_4$ using the GGA method.

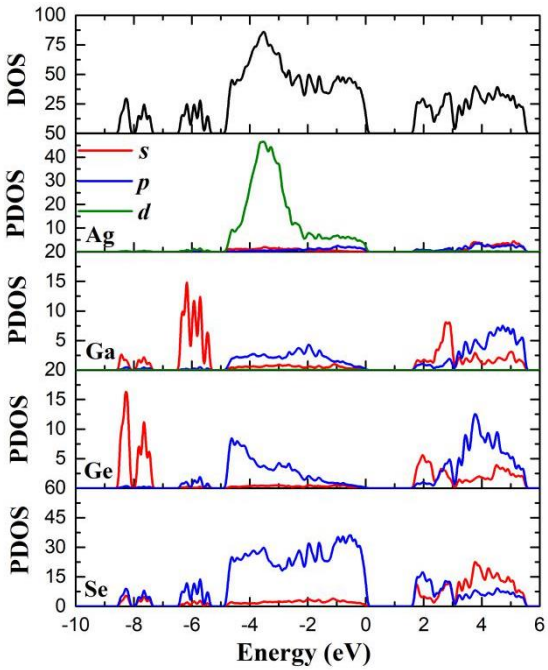

Figure 5. The partial density of states projected on respective atoms in $AgGaGeSe_4$ using the GGA method.

The first-principle-calculation of the refractive index in $AgGaGeSe_4$ was performed by the plane-wave pseudopotential method implemented in the CASTEP [44] package based on the density functional theory (DFT) [45,46]. The Perdew–Burk–Ernzerhorf (PBE) function of the general gradient approximation (GGA) form was used to describe the exchange-correlation energy [47–49]. The kinetic energy cutoff 650 eV and intensive Monkhorst–Pack [51] k-points $2 \times 2 \times 2$ mesh guarantee the reliability of our calculating results. The refractive index (n) was determined using the Kramers–Kronig transform [52]. Calculate the polarization spectra of the optical dielectric function; Figure S6 is the real part ε_1 of the dielectric function of $AgGaGeSe_4$, and Figure S7 is the imaginary part ε_2 of the dielectric function of $AgGaGeSe_4$. The results showed that the optical birefringence of the crystal is $\Delta n > 0.03$ (as shown in Figure 6), greater than the birefringence of $AgGaSe_2$ ($\Delta n = 0.02$), and phase matching can be achieved at 3000 nm to meet the phase-matching conditions of SHG in the IR region. In further research, we will try to synthesize large and high-quality $AgGaGeSe_4$ single crystals and measure their birefringence.

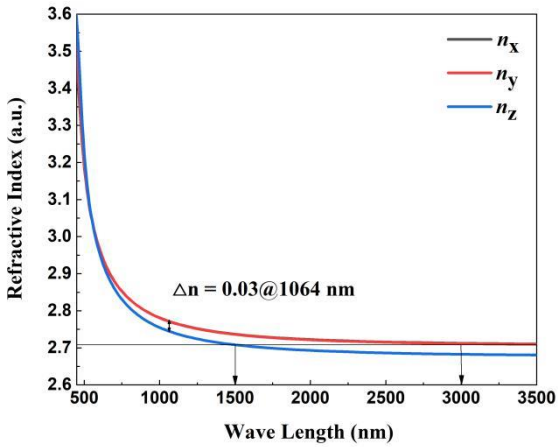

Figure 6. The calculated refractive index of $AgGaGeSe_4$.

4. Conclusions

In this paper, the $AgGaGeSe_4$ crystal with a tetragonal chalcopyrite structure was synthesized by introducing lighter Group IV Ge elements to the crystal of $AgGaSe_2$. In the $AgGaGeSe_4$ structure, Ge^{4+} replaces Ga^{3+} to produce an equal number of vacancies at the Ag^+ position. $AgSe_4$ and $(Ge/Ga)Se_4$ tetrahedrons were connected by common vertices to form a three-dimensional frame structure. From the diffuse reflection spectrum, the band gap width of $AgGaGeSe_4$ increased from 1.79 eV of $AgGaSe_2$ to 2.27 eV. The introduction of light Group IV Ge elements into the crystal structure of $AgGaSe_2$ effectively improves the band gap of $AgGaGeSe_4$. According to the calculated PDOS diagram analysis, the optical performance parameters of the $AgGaGeSe_4$ crystal largely depend on the Ag-Se and (Ge/Ga)-Se groups. The structural calculation showed that in the 1064 nm wavelength, the birefringence of $AgGaGeSe_4$ is 0.03, which is greater than that of $AgGaSe_2$ (Δn = 0.02). In addition, $AgGaGeSe_4$ has an SHG effect comparable to $AgGaSe_2$. The low content of Group IV Ge doping maintains its original chalcopyrite structure and improves its band gap and other optical properties. Therefore, compared with the traditional $AgGaSe_2$ crystal materials, many properties of the $AgGaGeSe_4$ crystal have been significantly improved. The addition of the Ge element not only improves the band gap of the material but also improves the birefringence of the material. A large band gap helps to enhance the laser damage threshold of the crystal and improve its transmittance to avoid two-photon absorption. Therefore, $AgGaGeSe_4$ is an excellent new infrared nonlinear optical material with great potential for application in infrared nonlinear optics.

Supplementary Materials: The following supporting information can be downloaded at: https://www.mdpi.com/article/10.3390/sym14071426/s1. Figure S1: EDS analyses of $AgGaGeSe_4$; Figure S2: XPS survey scan data of $AgGaGeSe_4$; Figure S3: Tauc plot of direct band gap in $AgGaGeSe_4$; Figure S4: The SHG intensity of a $AgGaGeSe_4$ sample compared to that of $AgGaSe_2$ using a 2.0 μm laser; Figure S5: The calculated band structure of $AgGaGeSe_4$ using the local density approximation (LDA) Ceperley–Alder (CA) approach; Figure S6: The real part ε1 of dielectric function of $AgGaGeSe_4$; Figure S7: The imaginary part ε2 of dielectric function of $AgGaGeSe_4$; Table S1: Crystallographic data and details of structure refinement for $AgGaGeSe_4$; Table S2: Selected bond lengths (Å) and angles (deg) of $AgGaGeSe_4$; Table S3: Binding energy values of constituent element core-level electrons of $AgGaGeSe_4$.

Author Contributions: Conceptualization, J.D. and D.M.; theoretical calculation, N.W. and Z.L.; writing—original draft preparation, J.D.; writing—review and editing, J.D. and D.M.; and supervision, D.M., J.Y. and Y.W. All authors have read and agreed to the published version of the manuscript.

Funding: This research was funded by the National Natural Science Foundation of China (51972208).

Institutional Review Board Statement: Not applicable.

Informed Consent Statement: Not applicable.

Data Availability Statement: CCDC 2151148 contains the supplementary crystallographic data for this paper. These data can be obtained free of charge via www.ccdc.cam.ac.uk/data_request/cif or by emailing data_request@ccdc.cam.ac.uk. Other data generated or analyzed during this study are included in this published article.

Conflicts of Interest: The authors declare no conflict of interest.

References

1. Guo, S.P.; Chi, Y.; Guo, G.C. Recent achievements on middle and far-infrared second-order nonlinear optical materials. *Coord. Chem. Rev.* **2017**, *335*, 44–57. [CrossRef]
2. Rosemann, N.W.; Eubner, J.P.; Beyer, A.; Koch, S.W.; Volz, K.; Dehnen, S.; Chatterjee, S. A highly efficient directional molecular white-light emitter driven by a continuous-wave laser diode. *Science* **2016**, *352*, 1301–1304. [CrossRef] [PubMed]
3. Wu, Q.; Yang, C.; Liu, X.; Ma, J.; Liang, F.; Du, Y.S. Dimensionality reduction made high-performance mid-infrared nonlinear halide crystal. *Mater. Today Phys.* **2021**, *21*, 100569. [CrossRef]
4. Lin, H.; Wei, W.B.; Chen, H.; Wu, X.T.; Zhu, Q.L. Rational design of infrared nonlinear optical chalcogenides by chemical substitution. *Coord. Chem. Rev.* **2020**, *406*, 213150. [CrossRef]
5. Wang, W.K.; Mei, D.J.; Liang, F.; Zhao, J.; Wu, Y.D.; Lin, Z.S. Inherent laws between tetrahedral arrangement pattern and optical performance in tetrahedron-based mid-infrared nonlinear optical materials. *Coord. Chem. Rev.* **2020**, *421*, 213444. [CrossRef]
6. Wang, W.K.; Mei, D.J.; Wen, S.G.; Wang, J.; Wu, Y.D. Complex coordinated functional groups: A great genes for nonlinear optical materials. *Chin. Chem. Lett.* **2021**, *33*, 2301–2315. [CrossRef]
7. Boyd, G.; Kasper, H.; McFee, J. Linear and nonlinear optical properties of $AgGaS_2$, $CuGaS_2$, and $CuInS_2$, and theory of the wedge technique for the measurement of nonlinear coefficients. *IEEE J. Quantum Electron.* **1971**, *7*, 563–573. [CrossRef]
8. Zhu, S.; Liu, J.; Zhao, B.; Jiang, H.; Li, Z. Crystal Growth and Differential Thermal Analysis of $AgGaSe_2$. *Cryst. Res. Technol.* **1995**, *30*, 1165–1168. [CrossRef]
9. Boyd, G.D.; Buehler, E.; Storz, F.G. Linear and nonlinear optical properties of $ZnGeP_2$ and CdSe. *Appl. Phys. Lett.* **1971**, *18*, 301–304. [CrossRef]
10. Li, W.K.; Li, Y.Y.; Xu, Y.; Lu, J.; Wang, P.F.; Du, J.; Leng, Y.X. Measurements of nonlinear refraction in the mid-infrared materials $ZnGeP_2$ and $AgGaS_2$. *Appl. Phys. B* **2017**, *123*, 82. [CrossRef]
11. Tell, B.; Kasper, H.M. Optical and Electrical Properties of $AgGaS_2$ and $AgGaSe_2$. *Phys. Rev. B* **1971**, *4*, 4455–4459. [CrossRef]
12. Cao, W.Z.; Mei, D.J.; Yang, Y.; Wu, Y.W.; Zhang, L.Y.; Wu, Y.D.; He, X.; Lin, Z.S.; Huang, F.Q. From $CuFeS_2$ to $Ba_6Cu_2FeGe_4S_{16}$: Rational band gap engineering achieves large second-harmonicgeneration together with high laser damage threshold. *Chem. Commun.* **2019**, *55*, 14510–14513. [CrossRef] [PubMed]
13. Kang, L.; Zhou, M.L.; Yao, J.Y.; Lin, Z.S.; Wu, Y.C.; Chen, C.T. Metal thiophosphates with good mid-infrared nonlinear optical performances: A first-principles prediction and analysis. *J. Am. Chem. Soc.* **2015**, *137*, 13049–13059. [CrossRef]
14. Chung, I.; Kim, M.G.; Jang, I.; He, J.Q.; Ketterson, J.B.; Kanatzidis, M.G. Strongly nonlinear optical chalcogenide thin films of $APSe_6$ (A = K, Rb) from spin-coating. Angew. *Chem. Int. Ed.* **2011**, *50*, 10867–10870. [CrossRef]
15. Yu, H.W.; Young, J.S.; Wu, H.P.; Zhang, W.G.; Rondinelli, J.M.; Halasyamani, P.S. Electronic, crystal chemistry, and nonlinear optical property relationships in the dugganite $A_3B_3CD_2O_{14}$ Family. *J. Am. Chem. Soc.* **2016**, *138*, 4984–4989. [CrossRef]
16. Yin, W.L.; Iyer, A.K.; Li, C.; Yao, J.Y.; Mar, A. Noncentrosymmetric chalcogenides $BaZnSiSe_4$ and $BaZnGeSe_4$ featuring one-dimensional structures. *J. Alloys Compd.* **2017**, *708*, 414–421. [CrossRef]
17. Hou, F.J.; Mei, D.J.; Zhang, Y.L.; Liang, F.; Wang, J.; Lu, J.; Lin, Z.S.; Wu, Y.D. $SrZnSnSe_4$: A quaternary selenide with large second harmonic generation and birefringence. *J. Alloys Compd.* **2022**, *904*, 163944. [CrossRef]
18. Singh, N.B.; Knuteson, D.J.; Kanner, G.; Berghmans, A.; Green, K.; Wagner, B.; Kahler, D.; King, M.; McLaughlin, S. Ternary and quaternary selenide crystals for nonlinear optical applications. *Photon. Fib. Cryst. Dev.* **2011**, *8120*, 812002. [CrossRef]
19. Mei, D.J.; Cao, W.Z.; Wang, N.Z.; Jiang, X.X.; Zhao, J.; Wang, W.K.; Dang, J.H.; Zhang, S.Y.; Wu, Y.D.; Rao, P.H.; et al. Breaking through the "3.0 eV wall" of energy band gap in mid-infrared nonlinear optical rare earth chalcogenides by charge-transfer engineering. *Mater. Horiz.* **2021**, *8*, 2330–2334. [CrossRef]
20. Wu, J.; Huang, W.; Liu, H.G.; He, Z.Y.; Chen, B.J.; Zhu, S.F.; Zhao, B.J.; Lei, Y.X.; Zhou, X.N. Investigation on Thermal Properties and Crystal Growth of Nonlinear Optical Crystal $AgGaS_2$ and $AgGaGeS_4$. *Cryst. Growth Des.* **2020**, *20*, 3140–3153. [CrossRef]
21. Huang, W.; He, Z.Y.; Zhao, B.J.; Zhu, S.F.; Chen, B.J.; Wu, Y. Effect of Thermal Annealing Treatment and Defect Analysis on $AgGaGeS_4$ Single Crystals. *Inorg. Chem.* **2019**, *58*, 10846–10855. [CrossRef] [PubMed]
22. Guo, S.P.; Chi, Y.; Xue, H.G. $SnI_4(S_8)_2$: A novel adduct-type infrared second-order nonlinear optical crystal. *Angew. Chem. Int. Ed.* **2018**, *57*, 11540–11543. [CrossRef]
23. Liu, B.W.; Jiang, X.M.; Zeng, H.Y.; Guo, G.C. $[ABa_2Cl][Ga_4S_8]$ (A = Rb, Cs): Wide-spectrum nonlinear optical materials obtained by polycation-substitution-induced nonlinear optical (NLO)-functional motif ordering. *J. Am. Chem. Soc.* **2020**, *142*, 10641–10645. [CrossRef] [PubMed]
24. Yang, C.; Liu, X.; Teng, C.; Cheng, X.; Liang, F.; Wu, Q. Hierarchical molecular design of high-performance infrared nonlinear Ag_2HgI_4 material by defect engineering strategy. *Mater. Today Phys.* **2021**, *19*, 100432. [CrossRef]

25. Zhou, H.M.; Xiong, L.; Chen, L.; Wu, L.M. Dislocations that decrease size mismatch within the lattice leading to ultrawide band gap, large second-order susceptibility, and high nonlinear optical performance of $AgGaS_2$. *Angew. Chem. Int. Ed.* **2019**, *58*, 9979–9983. [CrossRef]
26. Kim, W.T. Optical properties of undoped and cobalt-doped IB-Ga-IVA-Se_4 single crystals. *Phys. Rev. B* **1991**, *44*, 8667–8671. [CrossRef]
27. Goodchild, R.G.; Hughes, O.H.; Lopez-Rivera, S.A.; Woolle, J.C. Energy gap values by optical absorption in I III IV Se_4 compounds. *Can. J. Phys.* **1982**, *60*, 1096–1100. [CrossRef]
28. Guo, S.P.; Cheng, X.Y.; Sun, Z.D.; Chi, Y.; Liu, B.W.; Jiang, X.M.; Li, S.F.; Xue, H.G.; Deng, S.Q.; Duppel, V.; et al. Large second harmonic generation (SHG) effect and high laser-induced damage threshold (LIDT) observed coexisting in gallium selenide. *Angew. Chem. Int. Ed.* **2019**, *131*, 8171–8175. [CrossRef]
29. Abudurusuli, A.L.J.; Huang, J.B.; Wang, P.; Yang, Z.H.; Pan, S.L.; Li, J.J. $Li_4MgGe_2S_7$: The First Alkali and Alkaline-Earth Diamond-Like Infrared Nonlinear Optical Material with Exceptional Large Band Gap. *Angew. Chem. Int. Ed.* **2021**, *60*, 24131–24136. [CrossRef]
30. Jiang, X.M.; Lin, S.J.; He, C.; Liu, B.W.; Guo, G.C. Uncovering functional motif of nonlinear optical material by insitu electron density and wavefunction studies under laser irradiation. *Angew. Chem. Int. Ed.* **2021**, *60*, 11799–11803. [CrossRef]
31. Wu, K.; Zhang, B.B.; Yang, Z.H. New Compressed Chalcopyrite-like $Li_2BaMIVQ_4$ (MIV = Ge, Sn; Q = S, Se): Promising Infrared Nonlinear Optical Materials. *J. Am. Chem. Soc.* **2017**, *139*, 14885–14888. [CrossRef] [PubMed]
32. Wu, K.; Pan, S.L. A review on structure-performance relationship toward the optimal design of infrared nonlinear optical materials with balanced performances. *Coord. Chem. Rev.* **2018**, *377*, 191–208. [CrossRef]
33. Mei, D.J.; Yin, W.L.; Feng, K.; Lin, Z.S.; Bai, L.; Yao, J.Y.; Wu, Y.C. $LiGaGe_2Se_6$: A new IR nonlinear optical material with low melting point. *Inorg. Chem.* **2012**, *51*, 1035–1040. [CrossRef] [PubMed]
34. Zhao, J.; Mei, D.J.; Wang, W.K.; Wu, Y.D.; Xue, D.F. Recent advances in nonlinear optical rare earth structures. *J. Rare Earths* **2021**, *39*, 1455–1466. [CrossRef]
35. Dang, J.H.; Mei, D.J.; Wu, Y.D.; Lin, Z.S. A comprehensive survey on nonlinear optical phosphates: Role of multicoordinate groups. *Coord. Chem. Rev.* **2021**, *431*, 213692. [CrossRef]
36. Myronchuk, G.L.; Lakshminarayana, G.; Kityk, I.V.; Fedorchuk, A.O.; Vlokh, R.O.; Kozer, V.R.; Parasyuk, O.V.; Piasecki, M. $AgGaGeS_4$ crystal as promising optoelectronic material. *Chalcogenide Lett.* **2018**, *15*, 151–156. Available online: https://www.researchgate.net/publication/324132099 (accessed on 18 January 2022).
37. Krymus, A.S.; Kityk, I.V.; Demchenko, P.; Parasyuk, O.V.; Myronchuk, G.L.; Khyzhun, O.Y.; Piasecki, M. $AgGaSiSe_4$: Growth, crystal and band electronic structure, optoelectronic and piezoelectric properties. *Mater. Res. Bull.* **2017**, *95*, 177–184. [CrossRef]
38. Mei, D.J.; Gong, P.F.; Lin, Z.S.; Feng, K.; Yao, J.Y.; Huang, F.Q.; Wu, Y.C. $Ag_3Ga_3SiSe_8$: A new infrared nonlinear optical material with a chalcopyrite structure. *CrystEngComm* **2014**, *16*, 6836–6840. [CrossRef]
39. Petrov, V.; Noack, F.; Badikov, V.; Shevyrdyaeva, G.; Panyutin, V.; Chizhikov, V. Phase-matching and femtosecond difference-frequency generation in the quaternary semiconductor $AgGaGe_5Se_{12}$. *Appl. Opt.* **2004**, *43*, 4590–4597. [CrossRef]
40. Huang, W.; Wu, J.; Chen, B.J.; Li, J.P.; He, Z.Y. Crystal Growth and Thermal Annealing of $AgGaGe_5Se_{12}$ Crystal. *J. Alloys Compd.* **2021**, *862*, 158002–158022. [CrossRef]
41. Hughes, O.H.; Woolley, J.C.; Lopez-Rivera, S.A.; Pamplin, B.R. Quaternary Adamantine Selenides and Tellurides of the Form I III IV VI_4. *Solid State Commun.* **1980**, *35*, 573–575. [CrossRef]
42. Sheldrick, G.M. A short history of SHELX. *Acta Cryst.* **2008**, *64*, 112–122. [CrossRef] [PubMed]
43. Sheldrick, G.M. Crystal structure refinement with SHELXL. *Acta Cryst.* **2015**, *71*, 3–8. [CrossRef]
44. Clark, S.J.; Segall, M.D.; Pickard, C.J.; Hasnip, P.J.; Probert, M.I.J.; Refson, K.; Payne, M.C. First principles methods using CASTEP. *Z. Kristallogr.* **2005**, *220*, 567–570. [CrossRef]
45. Kohn, W.; Sham, L.J. Self-Consistent Equations Including Exchange and Correlation Effects. *Phys. Rev.* **1965**, *140*, A1133–A1138. [CrossRef]
46. Payne, M.C.; Teter, M.P.; Allan, D.C.; Arias, T.A.; Joannopoulos, J.D. Iterative minimization techniques forab initiototal-energy calculations: Molecular dynamics and conjugate gradients. *Rev. Mod. Phys.* **1992**, *64*, 1045–1097. [CrossRef]
47. Reshak, A.H.; Parasyuk, O.V.; Fedorchuk, A.O.; Kamarudin, H.; Auluck, S.; Chyský, J. Optical Spectra and Band Structure of $AgxGaxGe_{1-x}Se_2$ (x = 0.333, 0.250, 0.200, 0.167) Single Crystals: Experiment and Theory. *J. Phys. Chem. B* **2013**, *117*, 15220–15231. [CrossRef]
48. Perdew, J.P.; Burke, K.; Ernzerhof, M. Generalized Gradient Approximation Made Simple. *Phys. Rev. Let.* **1996**, *77*, 3865–3868. [CrossRef]
49. Perdew, J.P.; Wang, Y. Accurate and simple analytic representation of the electron-gas correlation energy. *Phys. Rev. B* **1992**, *45*, 13244–13249. [CrossRef]
50. Hamann, D.R.; Schlüter, M.; Chiang, C. Norm-Conserving Pseudopotentials. *Phys. Rev. Lett.* **1979**, *43*, 1494–1497. [CrossRef]
51. Monkhorst, H.J.; Pack, J.D. Special points for Brillouin-zone integrations. *Phys. Rev. B* **1976**, *13*, 5188–5192. [CrossRef]
52. Zhang, Y.; Islam, Z.; Ren, Y.; Parilla, P.A.; Ahrenkiel, S.P.; Lee, P.L. Zero thermal expansion in a nanostructured inorganic-organic hybrid crystal. *Phy. Rev. Lett.* **2007**, *99*, 215901. [CrossRef] [PubMed]
53. Badikov, V.V.; Tyulyupa, A.G.; Shevyrdyaeva, G.S.; Sheina, S.G. Solid solutions in the $AgGaS_2$-GeS_2 and $AgGaSe_2$-$GeSe_2$ systems. *Inorg. Mater.* **1991**, *27*, 177–180.

54. Cheng, W.D.; Lin, C.S.; Luo, Z.Z.; Zhang, H. Designing the syntheses and photophysical simulations of noncentrosymmetric compounds. *Inorg. Chem. Front.* **2015**, *2*, 95–107. [CrossRef]
55. BullSchevciw, O.; White, W.B. The optical absorption edge of rare earth sesquisulfides and alkaline earth-rare earth sulfides. *Mater. Res. Bull.* **1983**, *18*, 1059–1068. [CrossRef]
56. Zhao, J.; Mei, D.J.; Yang, Y.; Cao, W.Z.; Liu, C.; Wu, Y.D.; Lin, Z.S. $Rb_{10}Zn_4Sn_4S_{17}$: A Chalcogenide with Large Laser Damage Threshold Improved from the Mn-Based Analogue. *Inorg. Chem.* **2019**, *52*, 15029–15033. [CrossRef]